RESEARCH ARTICLE

**ADVANCED
ENERGY & SUSTAINABILITY
RESEARCH**
Open Access

www.advenergysustres.com

Doped Conjugated Polymer Enclosing a Redox Polymer: Wiring Polyquinones with Poly(3,4-Ethylenedioxythiophene)

Fatima Nadia Ajjan, Ziyauddin Khan, Sergi Riera-Galindo, Samuel Lienemann, Mikhail Vagin, Ioannis Petsagkourakis, Roger Gabrielsson, Slawomir Braun, Mats Fahlman, Olle Inganäs, Magnus Berggren, and Xavier Crispin*

The mass implementation of renewable energies is limited by the absence of efficient and affordable technology to store electrical energy. Thus, the development of new materials is needed to improve the performance of actual devices such as batteries or supercapacitors. Herein, the facile consecutive chemically oxidative polymerization of poly(1-amino-5-chloroanthraquinone) (PACA) and poly(3,4-ethylenedioxythiophene (PEDOT) resulting in a water dispersible material PACA-PEDOT is shown. The water-based slurry made of PACA-PEDOT nanoparticles can be processed as film coated in ambient atmosphere, a critical feature for scaling up the electrode manufacturing. The novel redox polymer electrode is a nanocomposite that withstands rapid charging (16 A g^{-1}) and delivers high power (5000 W kg^{-1}). At lower current density its storage capacity is high (198 mAh g^{-1}) and displays improved cycling stability (60% after 5000 cycles). Its great electrochemical performance results from the combination of the redox reversibility of the quinone groups in PACA that allows a high amount of charge storage via Faradaic reactions and the high electronic conductivity of PEDOT to access to the redox-active sites. These promising results demonstrate the potential of PACA-PEDOT to make easily organic electrodes from a water-coating process, without toxic metals, and operating in non-flammable aqueous electrolyte for large scale pseudocapacitors.

1. Introduction

The demand for tailor-made and high-performing energy storage devices has triggered the development of new electrodes with high-specific energy and power, long-term cycling stability, and that exhibit minimal environmental impact at the same time possible to produce at low cost. Organic electrode materials possess remarkable electrochemical performance, show favorable characteristics possible to achieve via multifaceted synthetic pathways, while being abundant and relatively inexpensive to produce and process.[1–6] Thus, they have been rapidly developed in recent years as a new versatile platform for a wide variety of different energy storage devices such as supercapacitors, and for lithium-ion, sodium-ion, and multivalent-ion-based batteries.[7–18]

Conducting polymers are attractive as electrode materials due to their intrinsic conductivity in combination with reversible redox activity. However, the charge capacity of conducting polymers is usually relatively low because of charge repulsion from delocalized polarons and bipolarons on the polymer backbone and heavy monomer units.[19,20] This combined drawback effect is relatively more pronounced for poly(3,4-ethylenedioxythiophene) (PEDOT) compared to other derivatives of polythiophene, and with polypyrrole and polyaniline.[21,22] Nevertheless, PEDOT has been widely studied as a supercapacitor electrode material because it can work in a comparatively wider potential window and possesses high chemical stability in different environments, including acids.[23–27] To enhance the charge-storing response of PEDOT, its amalgamation with conjugated redox carbonyl polymers containing for instance quinones, imides, and/or active phenols functional groups that provide multielectron redox reactions is crucial to complement with rapid and reversible electrochemistry.[28–34] In particular, quinones can either be part of the chemical polymer backbone, covalently attached to the conductive backbone, or interconnected through electrostatic interactions or hydrogen bonding.[35–40] Thus, these conjugated redox polymers offer advantages to improve charge storage capacity and long-term stability by avoiding their dissolution into electrolytes, which can cause a decrease in the rate performance and cyclic stability.

Dr. F. N. Ajjan, Dr. Z. Khan, Dr. S. Riera-Galindo, S. Lienemann, Dr. M. Vagin, Dr. I. Petsagkourakis, Dr. R. Gabrielsson, Dr. S. Braun, Prof. M. Fahlman, Prof. M. Berggren, Prof. X. Crispin
Laboratory of Organic Electronics
Department of Science and Technology (ITN)
Linköping University
SE-601 74 Norrköping, Sweden
E-mail: xavier.crispin@liu.se

Prof. O. Inganäs
Biomolecular and Organic Electronics IFM
Linköping University
S-581 83 Linköping, Sweden

The ORCID identification number(s) for the author(s) of this article can be found under https://doi.org/10.1002/aesr.202000027.

Several articles have previously reported on the usefulness of polyanthraquinones and polyaminoanthraquinone derivatives in vastly different applications such as in chemical sensors, the removal of heavy metal ions, catalysts, corrosion protection, optical and electrochromic devices.[41–45] There has been a recent resurgence of interest in this kind of organic polymers as the electrode materials for the next generation of energy storage systems.[46–52] Most of the reported studies are focusing on the performance of polyanthraquinones as electrode material for energy storage devices.[47,51,53–58] Although polyaminoanthraquinones provide promising energy density, they possess a low electrical conductivity, which limits the power density that can be extracted from the charge storage electrode. Combinations of polyaminoanthraquinones with PEDOT have been done in bilayer and multilayer format, with limits to scaling up.[59] In this article, we design a new facile synthetic strategy based on only two-step chemical oxidative polymerizations that generate a novel porous organic polymer nanocomposite based on poly (1-amino-5-chloroanthraquinone) (PACA) and PEDOT. The resulting microporous nanocomposite is composed of two interpenetrated networks, one of PEDOT matrix providing good electrical conductivity and one of nanopores promoting the ionic transport. The combination of those two interpenetrated networks leads to a fast transport of electrons and ions toward the PACA redox sites in the nanocomposite. Its morphological and electrochemical characteristics show excellent charging/discharging properties even at high-charging rate (16 A g^{-1}), a high-specific capacitance of 594 F g^{-1}, a high redox potential, and good cyclability.

2. Results and Discussion

The two-step synthesis of the water-dispersible PACA–PEDOT polymer is shown in **Scheme 1**. The first step is driven via chemical oxidative polymerization of 1-amino-5-chloroanthraquinone (ACA) monomer in the presence of an organic solvent (o-dichlorobenzene) and aqueous acid medium, using potassium chromate as oxidant, similar to a protocol previously reported.[43] Consecutively, the oxidative polymerization of 3,4-ethylenedioxythiophene (EDOT), in aqueous media, takes place in the presence of the previously polymerized PACA by using iron (III) chloride as the catalyst and sodium persulfate as oxidant, at room temperature. The ^{1}H NMR spectrum of the resulting hybrid polymer shows signals at δ: 7.16, 7.33, 7.52, 7.84, and 8.22 ppm that are attributed to the protons on the PACA, whereas the resonance at δ 4.16 ppm is assigned to the ethylene bridge protons on PEDOT (Figure S1, Supporting Information). The comparison of the resonances of PACA:PEDOT reveals a resulting ratio of 6:1. The Fourier-transform infrared spectroscopy spectra of PACA, PEDOT–tosylate, and PACA–PEDOT polymers are compared and shown in Figure S2, Supporting Information. The spectral features of the PACA and PEDOT–tosylate are like those reported previously and the structural vibrations observed in both overlap consistently with the PACA–PEDOT spectrum.[43,60] In addition, X-ray photoelectron spectroscopy (XPS) analysis was conducted and revealed the content of the elements C, O, S, N, and Cl atoms (Figure S3, Supporting Information). XPS clearly shows the presence of predominant C 1s peak at around 284.8 eV, a pronounced peak from O 1s near 532 eV, and a N 1s peak located at about 400 eV. Also, two signals corresponding to two chemical states of S 2p and Cl 2p are also found. Therefore, both PACA and PEDOT are present on the surface of the sample within the probing depth of the XPS ($\approx$100 Å). The atomic concentrations from C, O, S, N, and Cl are found to be 60%, 21%, 2%, 8%, and 3%, respectively. Since PACA has one Cl atom and one N atom per monomer, and PEDOT has one S atom per monomer, the lower contents of Cl and N (2–3%) compared to 8% of S indicate that the surface composition has close to four times more PEDOT than PACA. This suggests
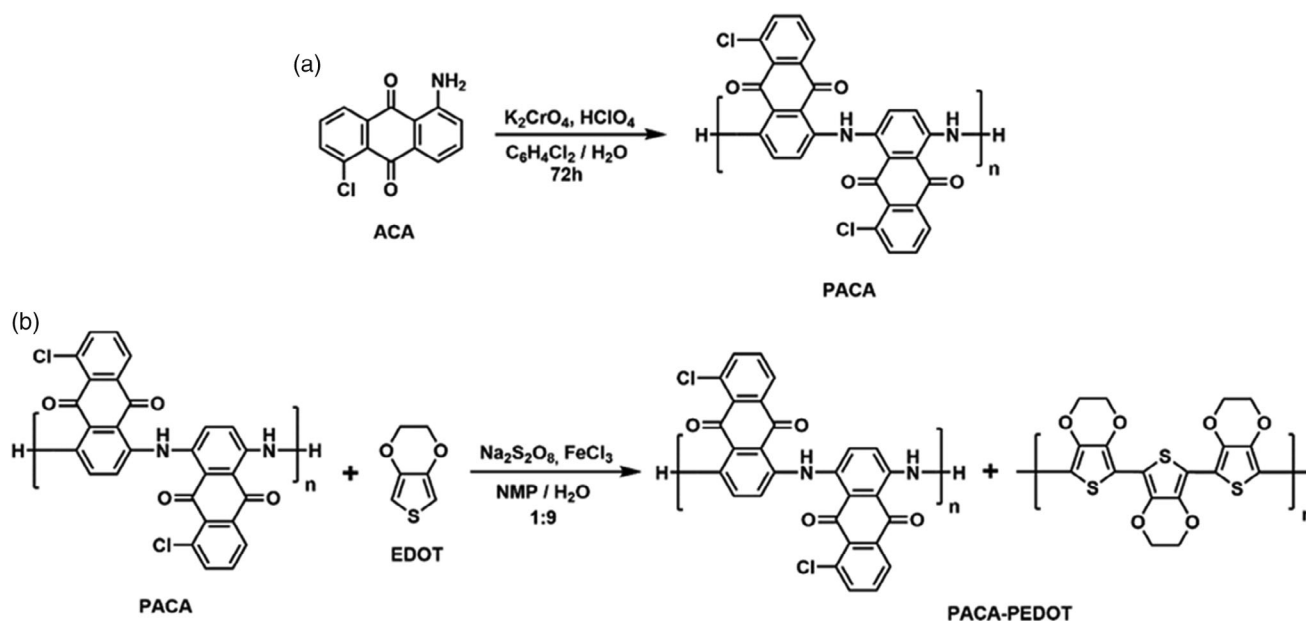
Scheme 1. Chemical oxidative polymerization of a) ACA and b) EDOT in the presence of PACA.

the formation of a PEDOT coating around PACA nanoparticles during the synthesis.

Dynamic light scattering (DLS) measurements were conducted to study the particle size of PACA and PACA–PEDOT in aqueous solutions showing 171 and 217 nm, respectively (Figure 3a). The hydrodynamic diameter in PACA–PEDOT composite increases ≈50 nm indicating a donor–acceptor interaction between the p-doped PEDOT, as a Lewis acid, and the electron pairs of the amino groups in PACA (**Figure 1**a). This increase in particle size together with the large PEDOT surface composition of films suggests that PEDOT deposits around the PACA nanoparticles during the polymerization of EDOT. Since the EDOT polymerization is oxidative, it is legitimate to wonder if the PACA nanoparticles are oxidized simultaneously to EDOT and if this can drive the deposition of PEDOT on the PACA nanoparticles. The UV–vis absorption spectrum of the polymerized PACA exhibits a band centered at 485 nm (Figure S4, Supporting Information), due to the quinone groups in the

anthraquinone rings. The reduction of PACA with $NaBHO_4$ shows the shift of the absorption peak to 420 nm corresponding to the reduced hydroquinone groups. On the contrary, there is an oxidation of PACA with K_2CrO_4 (oxidant in the medium of the polymerization of ACA) or with $FeCl_3$ (oxidant in the medium of the polymerization of EDOT) characterized by an absorption feature at shorter wavelength (365 nm) attributed to the quinoid state in the polymer backbone involved in an intramolecular charge transfer, in addition to a higher intensity band at nearly equal wavelength as PACA spectral feature (485 nm). This modification of the optical properties suggests that the PACA nanoparticles are oxidized during the polymerization of EDOT. We propose that the positively charged PACA nanoparticles surrounded by negative counterions at their surface promote the further deposition of positively charged PEDOT oligomers. This is a hypothesis for the mechanism of formation of PEDOT shells in this two-step polymerization synthesis. This might be a general mechanism which can open an interesting
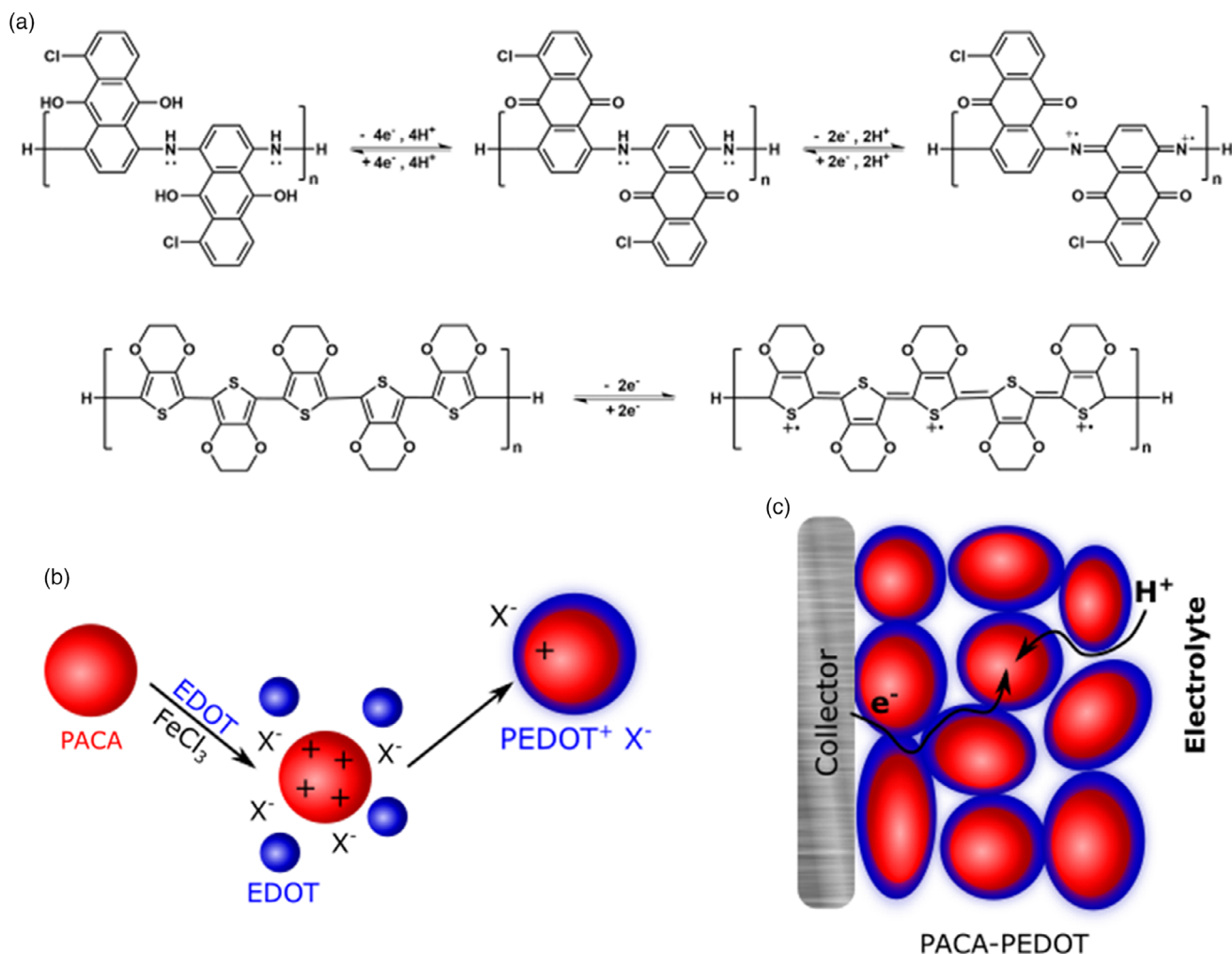

Figure 1. a) Redox states in the chemical structure of PACA and PEDOT showing the Faradaic reaction mechanism at the quinones and the π-conjugated system; b) scheme of oxidative polymerization of EDOT in presence of PACA, resulting in the final PACA–PEDOT composite; c) schematic illustration of electron transfer through the conductive PEDOT shell and the proton from the electrolyte till PACA site.

avenue for synthesizing efficient nanocomposites for polymer supercapacitors based on a redox (low-conducting polymer) and a highly conducting polymer shell.

The morphology of drop-casted PACA–PEDOT is characterized by scanning electron microscopy (SEM) (**Figure 2**b-c) and the elemental distribution was investigated by energy dispersive X-ray spectroscopy (EDX). SEM unveils a rough and extended microporous polymeric PACA–PEDOT composite. EDX confirms a successful complexation of PACA–PEDOT (Figure S6, Supporting Information) by revealing the homogenous presence of S, Cl, and N throughout the drop-casted material (probing depth of EDX is larger than XPS). The microporous morphology is created from the aggregation of nanoparticles of PACA–PEDOT during solvent evaporation and film formation. A high internal surface area of the microporous structure promotes fast ionic transport in the nanovoids filled of electrolyte, whereas the percolation path for the electronic charge carrier is maintained by the PEDOT shells. Both interpenetrating network of PEDOT and nanopores filled of electrolyte lead to efficient ion–electron charge transport toward the redox-active PACA material.

We have also characterized the electrical performance of spray-coated PACA–PEDOT films. The average sheet resistance is $497\,k\Omega\,sq^{-1}$, which decreases until $285\,k\Omega\,sq^{-1}$ after 50 h in ambient conditions (Figure S7, Supporting Information). The thickness of this film is $500 \pm 200\,nm$ and the conductivity is in the range of $0.2 \pm 0.1\,S\,cm^{-1}$. The Seebeck coefficient of the PACA–PEDOT composite is small and equals $4.5\,\mu V\,K^{-1}$. This value is lower than that found for typical PEDOT films (≈ 30–$50\,\mu V\,K^{-1}$),[61] thus indicating that PACA affects the transport properties of PEDOT in the nanocomposite while holes remain as majority charge carriers.

In situ resistometry was utilized to study the electrical behavior of the materials under electrochemical measurements.[62,63] The postmodification of PACA by highly conductive PEDOT results in a decrease in channel resistance more than four orders of magnitude (**Figure 3**). This underlines the distinctive role of PEDOT governing the electrical conductivity in the PACA–PEDOT composite. PEDOT is known to be one of the best conducting polymers with a conductivity up to 500–1500 S cm^{-1}.[61] Although PEDOT films displays a constant resistance extending to $-0.7\,V$ versus AgCl before undergoing major dedoping (reduction) accompanied by a significant rise in resistance,[60] the PACA–PEDOT composite behaves differently with a cup-shaped dependence and early rise in resistance already at 0 V. The rise in resistance at negative applied potentials manifests the reduction process of PEDOT ($PEDOT^{+}X^{-} + e^{-} \rightarrow PEDOT^{0} + X^{-}$, see Figure 1a),[64] which is affected by presence of PACA. This is a dynamic process, possibly limited by the ionic transport (leaving anions X^{-}) as indicated by different curves obtained at different scan rates. Note that increasing ten times the concentration of protons in the solution (from 0.1 M $HClO_4$ in Figure 3a to 1 M $HClO_4$ in Figure 3b) reveals yet another feature that is not observed in pure PEDOT films: in the voltage range attributed to the reduction of PACA [0 V; -0.2 V] ($PACA^{0} + 2\,H^{+} + 2e^{-} \rightarrow PACA\text{-}(OH)_2$, see Figure 1a), a bump is observed in the resistance evolution before the expected rise attributed to the PEDOT reduction. This "bump" is an indication of the interplay between the redox process in PACA involving protons captured from the electrolyte, and the electronic transport process in the composite dominated by the PEDOT nanophase. Therefore, this shows that PEDOT and PACA are intimately coupled
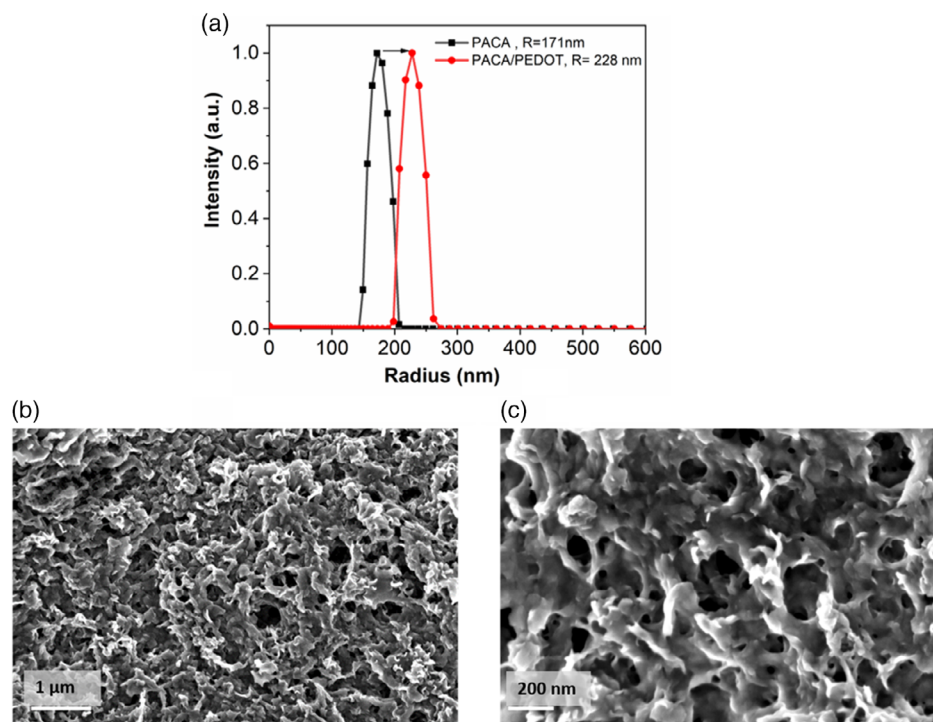

Figure 2. a) DLS of PACA (black) and PEDOT–PACA (red). SEM imaging of PACA–PEDOT b) 200 nm magnification and c) 1 μm magnification.

ADVANCED
SCIENCE NEWS
www.advancedsciencenews.com

ADVANCED
ENERGY & SUSTAINABILITY
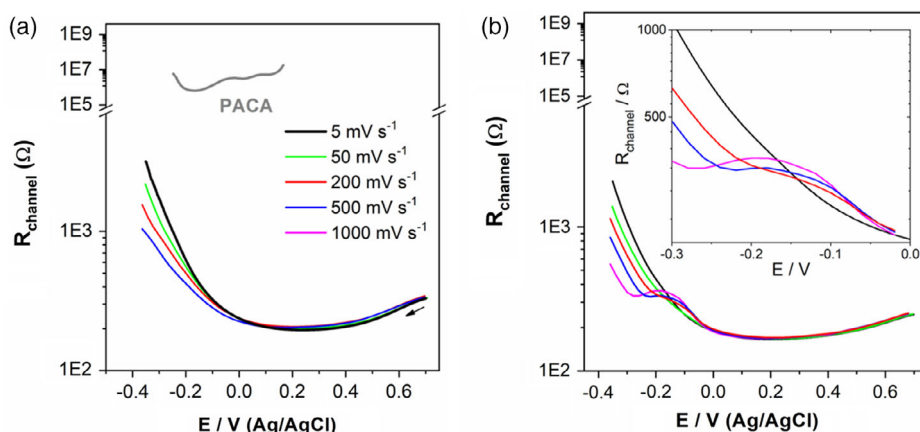RESEARCH
Open Access
www.advenergysustres.com

Figure 3. Dedoping of PACA–PEDOT conducting polymer composite by PACA redox process. a,b) The dependencies of channel resistance on the applied voltage were obtained on PACA–PEDOT films drop-casted on gold interdigitated electrodes obtained in 0.1 M $HClO_4$ and 1 M $HClO_4$, respectively; Inset: zoomed region of (b).

likely at the molecular scale at the interface. It is indeed not excluded that PACA nanoparticles are swollen by solvent during the EDOT polymerization, so that an interpenetrating network between PACA nanoparticles and PEDOT shells is formed.

The electrochemical performance of this hybrid polymer electrode was evaluated by cyclic voltammetry (CV) and galvanostatic charge–discharge cycling using a three-electrode cell

configuration performed in an aqueous electrolyte solution (0.1 M perchloric acid). CVs of PACA–PEDOT (**Figure 4**a) at different scan rates (from 10 to 100 mV s^{-1}) in the potential range of from −0.4 to 0.8 V show very distinct oxidation and reduction peaks at negative and positive potentials. At negative potentials, from −0.4 to 0 V, the reversible oxidation and reduction peaks are attributed to Faradaic processes of the quinone moieties of PACA, whereas the capacitive character (square box of the
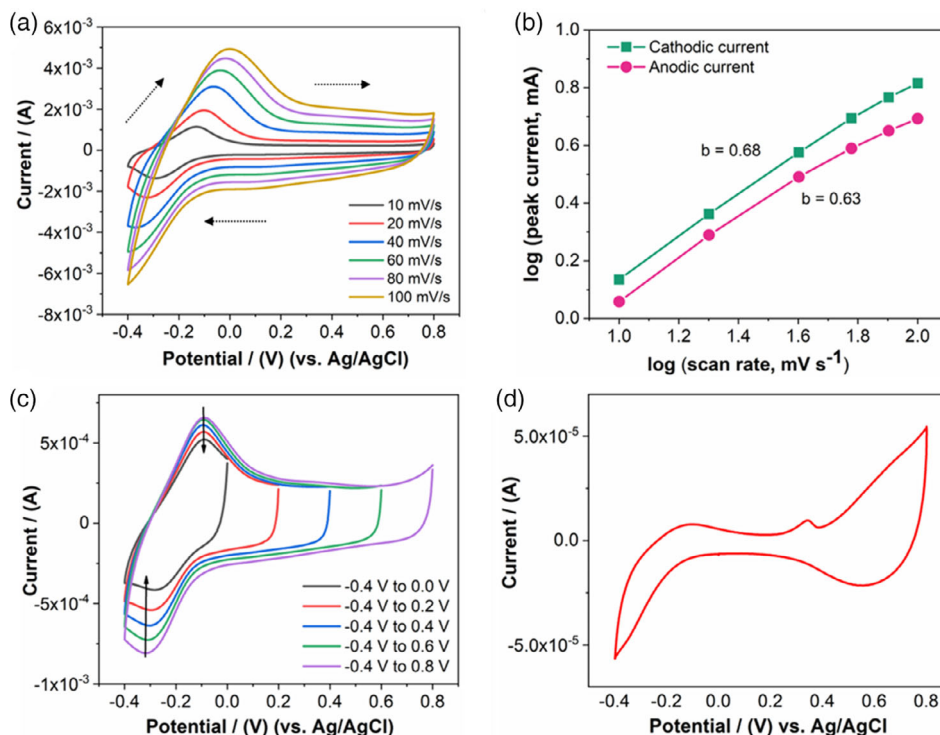

Figure 4. a) CV of PACA–PEDOT at different scan rates from 10 to 100 mV s^{-1}, the scan rate direction is indicated by black arrows; b) relationship between cathodic and anodic peak current with scan rates to estimate the Faradaic and nonFaradaic processes; c) CV at different potential ranges; and d) CV of PACA at 50 mV s^{-1}. These set of measurements were recorded in three-electrode cell configuration using 0.1 M $HClO_4$ electrolyte solution.

2000027 (5 of 9)

current–voltage characteristics) at positive potentials, from 0 to 0.8 V, is due to PEDOT. It was observed that the peak current increases with the scan rate, which suggests that the rate of electronic and ionic transports as well as kinetics of interfacial redox reactions is fast enough at a high sweep rate.[65] The charge storage mechanism in PACA–PEDOT whether capacitive or Faradaic can be analyzed by the relationship between measured current (i) and sweep rate (v) using power law $i = av^b$ where a and b are constants. The value of b can be obtained from the slope of graph plotted between log i versus log v which typically varies from 0.5 to 1. For nonFaradaic process, the value b is close to 1, whereas for Faradaic process, it is close to 0.5. The slope for log i versus log v was estimated to be 0.68 for cathodic peak currents and 0.63 for anodic peak currents (Figure 4b), and for both peaks, the value is approaching to 0.5 thus suggesting that the charge storage mechanism is dominated by surface-controlled diffusion process.[66,67] Interestingly, the large capacitive effect of the PEDOT phase and the reversible Faradaic process inherent to PACA strongly depend on the variation of the potential window applied (Figure 4c). Since CV is not a steady-state measurement, this observation reveals the competition between the kinetic of dedoping of PEDOT and kinetics of electron transfer for the Faradaic redox process within PACA. If both are of the same order of magnitude, it likely indicates that the limiting process for both phenomena is the ionic transport. This may suggest that an extended access to the aminoanthraquinone redox sites is established as PEDOT provides a relatively more conductive pathway when higher

positive potentials are applied. This then promotes faster and higher density of electron transfer within the material. Conversely, the protons become relatively more trapped within the reduced hydroquinone state of PACA as the PEDOT backbone becomes less conductive when the potential window is narrowed. This then decreases the electron transfer pathways between PEDOT and PACA. The electrochemical response of the PACA–PEDOT composite is very different from that of PEDOT and PACA alone. A significant difference is observed in the CV characteristics performed on only the PACA material (Figure 4d), which displays considerably lower current density, positive doping with capacitive behavior type on positive potentials, and a nonreversible cathodic contribution because there is an incomplete reduction peak involving the quinone groups at negative potentials (Figure S9, Supporting Information), thus proving the low conductivity of this conjugated redox polymer. Therefore, the amplified and reversible electrochemical reduction of PACA in the PACA–PEDOT composite is a clear indication of the intimate coupling between PEDOT and PACA and the interplay of their functions (electrical conductivity and redox behavior).

The fundamental charge storage performance of PACA–PEDOT is further analyzed with galvanostatic charge–discharge (GCD) analysis by applying different charging rates, ranging from 1 to 16 A g^{-1} estimated with respect to the weight of active electrode material (**Figure 5**a). The two different slopes confirm a change in the charge storage mechanisms by fully utilizing the pseudocapacitive redox processes of the composite material
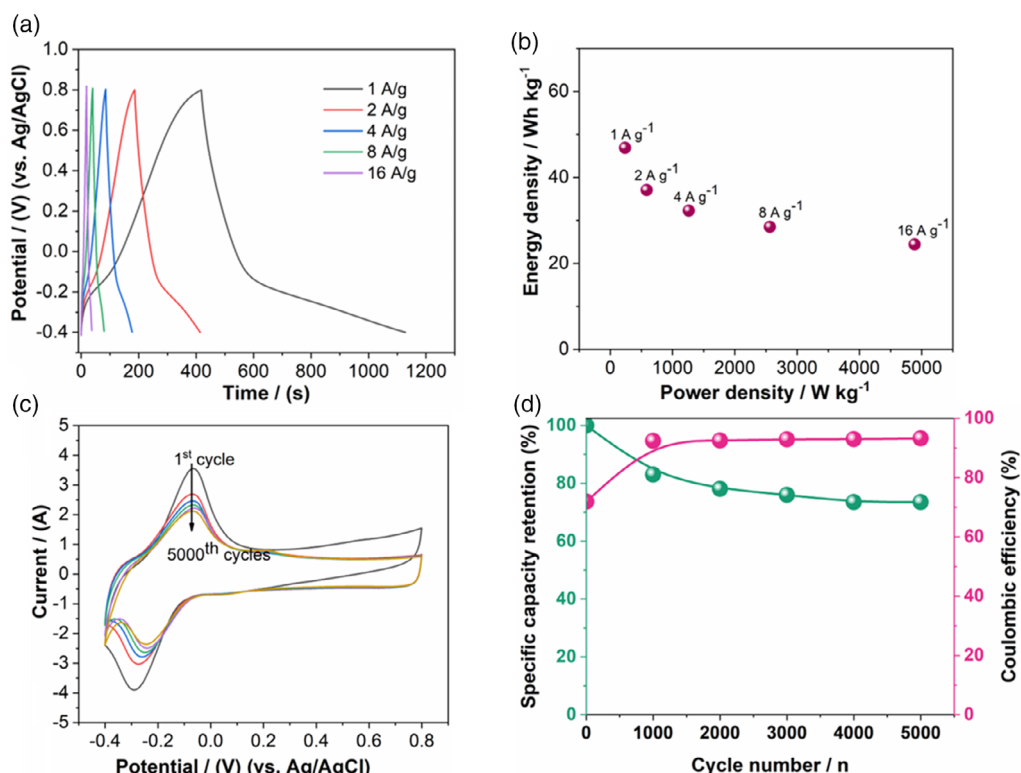

Figure 5. a) Galvanostatic charge–discharge profiles at different current densities from 1 to 16 A g^{-1}; b) Ragone plot at different current densities from 1 to 16 A g^{-1}; c) CV from the 1st to the 5000th cycle every 1000 cycles; and d) Coulombic efficiency and specific capacitance retention over 5000 cycles at a discharge current rate of 32 A g^{-1}.

system. Indeed, the first linear decay of the discharge from 0.8 to −0.1 V comes from the capacitive behavior of PEDOT; whereas the second slope from −0.1 to −0.4 V originates from the Faradaic process in PACA (see also Figure S11, Supporting Information). The specific capacitances of the supercapacitor electrodes are calculated from the slope of the discharge curves (Figure S10, Supporting Information), then obtaining a specific capacitance value of 594 F g^{-1} at 1 A g^{-1}. This value is in fact greater than the values reported in literature for comparable hybrid polymer materials.[46,47,59,68–71] The porous morphology is favorable for rapid ionic transport through nanopores filled with electrolyte and the presence of PEDOT in the composite provides a high holes conductivity, thus ensuring a fast redox-charging in PACA. We believe the unique morphology of the PACA–PEDOT electrode enables high rate capability as indicated by the slight decrease in charge capacity as the current rate increases. We further investigated the Ragone plot, which compares the energy and power densities of the hybrid polymer, see Figure 5b. PACA–PEDOT exhibited an energy density in the range of 46.8–24.4 Wh kg^{-1} and a power density ranging from 237.6 to 4887.6 W kg^{-1}, as the charging rate increases from 1 to 16 A g^{-1}. The energy density decreases with the increase in power density. In addition, the cycling stability was studied by continuously operating CV (Figure 5c) and galvanostatic charge/discharge at an elevated charge rate of 32 A g^{-1} for 5000 cycles (Figure 5d and S12, Supporting Information). Despite of the low-specific capacitance (79.2 F g^{-1}), PACA–PEDOT featured 60% capacity retention after 5000 cycles, indicating good stability of the material when cycled at high currents. The coulombic efficiency of the system was also estimated and found to increase from 72% to 93% after 5000 cycles, which suggests an improvement in the reversibility of redox processes (Figure 5d). Also, comparative voltammograms of PACA–PEDOT for 1st and 5000th cycle showed well-pronounced redox peaks related to PACA and a capacitive behavior attributed to PEDOT which suggests superior long-term stability of the polymer composite as an electrode (Figure 5c).

Self-discharge is always of fundamental interest in describing the behavior of electrochemical charge storage electrodes because it involves progressive and time-dependent loss of charge visible in a decrease in potential over time. Self-discharge of PACA–PEDOT was measured by monitoring the open-circuit voltage for 18 h under inert atmosphere, after charging to a potential of −0.4 V. As shown in Figure S13, Supporting Information, the hybrid polymer electrode undergoes a relatively fast initial self-discharging process, during the first 2 h at open-circuit conditions. Afterward, the change in open-circuit potential remains constant (linear decay) during the following hours without any sign of transient decrease.

3. Conclusion

The novel polymer nanocomposite electrode based on PEDOT and the polyaminoanthraquinone derivative, PACA, has been synthesized via a straightforward two-step oxidative polymerization protocol: one step to fabricate redox active PACA nanoparticles and a next step to coat PACA nanoparticles with the highly conducting PEDOT. This process results in a water dispersible electrode material with favorable morphology with the synergistic effects between the versatility of the quinone groups in PACA allowing high amount of electric charge storage via Faradaic reactions and PEDOT serving as an electronic conductor allowing easy access to the abundant redox-active sites. In addition, the PACA–PEDOT nanocomposite electrode is fabricated from a water slurry in air, a convenient feature for scaling up its manufacturing; moreover, it is operated in a nonflammable aqueous electrolyte, which will provide safety when integrated in an organic pseudocapacitor. The PACA–PEDOT nanocomposite electrode sustains high charge rates (16 A g^{-1}) and delivers high power (5000 W kg^{-1}). It also reaches high-specific capacitance (≈600 F g^{-1}), i.e., charging capacities of ≈200 mA h g^{-1} at lower charge rates, features that outperform the properties of the pristine electroactive polymers examined separately. Thus, the strategy of creating a microporous electrode from the deposition of core–shell polymer nanoparticles with a shell of conducting polymer and a core of redox polymer is an attractive route for the fabrication of organic pseudocapacitor electrode of high performance.

4. Experimental Section

Materials: EDOT (99%, Acros organics), sodium persulfate (Na$_2$S$_2$O$_8$), iron (III) chloride (FeCl$_3$), acetonitrile (MeCN), perchloric acid (HClO$_4$), ACA, potassium chromate (K$_2$CrO$_4$), o-dichlorobenzene (C$_6$H$_4$Cl$_2$), N-methyl-2-pyrrolidone (NMP) (Sigma-Aldrich) were used. All reagents and solvents were used as received. The aqueous solutions were prepared with ultrapure deionized water (Millipore).

Synthesis of PEDOT–PACA: The synthesis of PEDOT–PACA was conducted in a two-step chemical oxidative polymerization. First, the polymerization of ACA monomer for the synthesis of the PACA was conducted by following this procedure: ACA (5 mmol) and 70 % HClO$_4$ (8.8 mmol) were added to 30 mL of C$_6$H$_4$Cl$_2$ in a 100 mL conical flask in a water bath at 30 °C and then stirred vigorously for 20 min. An oxidant solution was prepared separately by dissolving the oxidant K$_2$CrO$_4$ (10 mmol) in a 5 mL of distilled water at 30 °C. The ACA monomer solution was then treated with the oxidant solution in one portion. The reaction mixture was magnetically and continuously stirred for 72 h at 30 °C. PACA polymer was isolated from the reaction mixture by centrifugation and washed with an excess of distilled water and ethanol to remove the residual oxidant, remaining monomer, and oligomers. The PACA polymer was dried at 60 °C in the oven for 2 days.

Second, the polymerization of EDOT, in the presence of PACA (weight ratio of 1:1 PACA:EDOT), was conducted in a solvent mixture of 9:1 deionized water:NMP, respectively, under ambient conditions. PACA was dissolved in NMP and then deionized water was added dropwise to this solution, continuing with the addition of EDOT under stirring. An oxidant solution was prepared separately by dissolving the oxidant Na$_2$S$_2$O$_8$ (1.6 equivalents) and FeCl$_3$ (1.6 equivalents). The oxidative polymerization was conducted under mechanical stirring at room temperature for 24 h. Finally, the obtained hybrid polymer material was dialyzed for 72 h using a 3.5–5 kD membrane and isolated by centrifugation. The overall yield of the polymerization was 75%.

Electrochemical Characterization: Three-Electrode Configuration Measurements: CV and GCD tests were recorded using Autolab PGStat 10 (Eco Chemie, the Netherlands). In the three-electrode system, platinum wire, Ag/AgCl (KCl sat.), and gold electrode (Au, with an area of 1.0 cm^2) were used as counter (CE), reference (RE), and working electrodes, respectively, (Bioanalytical Systems Inc. USA). The masses of the drop-casted films were weighed using a microanalytical balance with a mass of 580 µg cm^{-2}. All the electrochemical measurements were performed using freshly prepared 0.1 m HClO$_4$ aqueous solution as electrolyte.

**ADVANCED
SCIENCE NEWS**
www.advancedsciencenews.com

**ADVANCED
ENERGY & SUSTAINABILITY
RESEARCH**
Open Access
www.advenergysustres.com

Material Characterization: ^{1}H NMR analysis was recorded at 300 MHz using deuterated dimethyl sulfoxide $(CD_3)_2SO$) as solvent on a Varian Oxford 300 MHz spectrometer using internal solvent peaks as reference. NMR FID files were processed with MestReNova v12.04-22 023, 2018 Mestrelab Research S.L.

XPS was performed on an XPS spectrometer Scienta ESCA 200 (base pressure of 10^{-10} mbar, monochromatic Al (Kα) X-ray source, full width at half maximum of the clean Au4f$_{7/2}$ line $= 0.65$ eV, normal emission).

UV–Vis Spectroscopy: Spectra were acquired at room temperature on a fiber optic spectrometer (AvaSpec-NIR256-2.5-HSC-EVO).

Dynamic Light Scattering: PACA was suspended in NMP at 10 mg mL^{-1} and two different samples of PACA–PEDOT were suspended in NMP at 10 mg mL^{-1} in distilled H_2O at 3.3 mg mL^{-1}, respectively. All samples were measured in 10 mm diameter cylindrical cuvettes using a temperature controlled ($22 \pm 0.02\,°C$) and refractive index-matching toluene bath. An ALV-CGS-5022 F goniometer system (ALV GmbH, Langen) with a 22 mW 633 nm HeNe laser was used for the characterization, which was operated in pseudo–cross-correlation mode, with scattered light collected into a single-mode optical fiber and split to two avalanche photodiodes (Perkin-Elmer). A dual multiple-tau correlator with 328 channels (ALV-6010-160) was used to generate the time correlation. The correlation time distributions were then calculated through a constrained regularization method (CONTIN, supplied with the correlator software), whereas the Stokes–Einstein relationship was used to convert them into size distributions.[1] SEM and EDX were obtained using a Zeiss Sigma 500 Gemini scanning electron microscope with an acceleration voltage of 3 kV and a Bruker EDS XFlash6 with an acceleration voltage of 7 kV, respectively.

Spray-Coated Samples: All devices were fabricated on glass substrates cleaned sequentially in acetone, and isopropanol, dried with nitrogen flow. A 3 nm Cr and 20 nm of Au were thermally evaporated on the substrates defining a geometry of two separate electrodes ($L/W = 0.5$ mm/15 mm). PEDOT–PACA water dispersion was stirred before deposition and spray coated by means of a commercially available air brush on the top of the substrates kept at 150 °C on a hotplate. Sheet resistances were measured with Keithley 4200 using a four-point resistance probe (Signatone S-302). The Seebeck coefficients of the spray-coated films were measured applying a temperature gradient (ΔT) across the sample fixed by two Peltier modules. The thermal voltage (ΔV) was probed between two separate gold electrodes ($L/W = 0.5$ mm/15 mm). The Seebeck coefficient was obtained from the slope of ΔV measured at six different ΔT values.

Supporting Information

Supporting Information is available from the Wiley Online Library or from the author.

Conflict of Interest

The authors declare no conflict of interest.

[1] S. Muench, A. Wild, C. Friebe, B. Häupler, T. Janoschka, U. S. Schubert, *Chem. Rev.* **2016**, *116*, 9438.
[2] C. Liedel, X. Wang, M. Antonietti, *Nano Energy* **2018**, *53*, 536.
[3] S.-K. Kim, J. Cho, J. S. Moore, H. S. Park, P. V. Braun, *Adv. Funct. Mater.* **2016**, *26*, 903.
[4] A. Mukhopadhyay, Y. Jiao, R. Katahira, P. N. Ciesielski, M. Himmel, H. Zhu, *Nano Lett.* **2017**, *17*, 7897.
[5] D. Yiğit, M. Güllü, *J. Mater. Chem. A* **2017**, *5*, 609.
[6] X. Geng, Y. Zhang, L. Jiao, L. Yang, J. Hamel, N. Giummarella, G. Henriksson, L. Zhang, H. Zhu, *ACS Sustain. Chem. Eng.* **2017**, *5*, 3553.
[7] F. Wang, S. Xiao, Y. Hou, C. Hu, L. Liu, Y. Wu, *RSC Adv.* **2013**, *3*, 13059.
[8] L. Yu, G. Z. Chen, *J. Power Sources* **2016**, *326*, 604.
[9] X. Yue, H. Liu, P. Liu, *Chem. Commun.* **2019**, *55*, 1647.
[10] F. Wang, X. Fan, T. Gao, W. Sun, Z. Ma, C. Yang, F. Han, K. Xu, C. Wang, *ACS Cent. Sci.* **2017**, *3*, 1121.
[11] G. Wu, P. Tan, D. Wang, Z. Li, L. Peng, Y. Hu, C. Wang, W. Zhu, S. Chen, W. Chen, *Sci. Rep.* **2017**, *7*, 43676.
[12] A. M. Navarro-Suárez, N. Casado, J. Carretero-González, D. Mecerreyes, T. Rojo, *J. Mater. Chem. A* **2017**, *5*, 7137.
[13] F. Li, X. Wang, R. Sun, *J. Mater. Chem. A* **2017**, *5*, 20643.
[14] Z. Zhang, M. Liao, H. Lou, Y. Hu, X. Sun, H. Peng, *Adv. Mater.* **2018**, *30*, 1.
[15] T. Suga, H. Ohshiro, S. Ugita, K. Oyaizu, H. Nishide, *Adv. Mater.* **2009**, *21*, 1627.
[16] Y. Liang, Z. Tao, J. Chen, *Adv. Energy Mater.* **2012**, *2*, 742.
[17] M. Park, D. S. Shin, J. Ryu, M. Choi, N. Park, S. Y. Hong, J. Cho, *Adv. Mater.* **2015**, *27*, 5141.
[18] S. Gheytani, Y. Liang, F. Wu, Y. Jing, H. Dong, K. K. Rao, X. Chi, F. Fang, Y. Yao, *Adv. Sci.* **2017**, *4*, 1.
[19] J. Kim, J. H. Kim, K. Ariga, *Joule* **2017**, *1*, 739.
[20] A. M. Bryan, L. M. Santino, Y. Lu, S. Acharya, J. M. D'Arcy, *Chem. Mater.* **2016**, *28*, 5989.
[21] G. A. Snook, P. Kao, A. S. Best, *J. Power Sources* **2011**, *196*, 1.
[22] M. Boota, Y. Gogotsi, *Adv. Energy Mater.* **2019**, *9*, 1.
[23] T. Ahuja, I. Mir, D. Kumar, Rajesh, *Biomaterials* **2007**, *28*, 791.
[24] B. Anothumakkool, R. Soni, S. N. Bhange, S. Kurungot, *Energy Environ. Sci.* **2015**, *8*, 1339.
[25] S. Ghosh, O. Inganäs, *Adv. Mater.* **1999**, *11*, 1214.
[26] J. C. Carlberg, O. Inganäs, *J. Electrochem. Soc.* **1997**, *144*, L61.
[27] S. Ghosh, O. Inganäs, *J. Electrochem. Soc.* **2000**, *147*, 1872.
[28] Y. Liang, Y. Jing, S. Gheytani, K. Y. Lee, P. Liu, A. Facchetti, Y. Yao, *Nat. Mater.* **2017**, *16*, 841.
[29] Y. Wu, R. Zeng, J. Nan, D. Shu, Y. Qiu, S.-L. Chou, *Adv. Energy Mater.* **2017**, *7*, 1700278.
[30] G. Hernández, N. Casado, A. M. Zamarayeva, J. K. Duey, M. Armand, A. C. Arias, D. Mecerreyes, *ACS Appl. Energy Mater.* **2018**, *1*, 7199.
[31] N. Patil, A. Aqil, F. Ouhib, S. Admassie, O. Inganäs, C. Jérôme, C. Detrembleur, *Adv. Mater.* **2017**, *29*, 1.
[32] J. Y. Oh, Y. Jung, Y. S. Cho, J. Choi, J. H. Youk, N. Fechler, S. J. Yang, C. R. Park, *ChemSusChem* **2017**, *10*, 1644.
[33] M. Lee, J. Hong, B. Lee, K. Ku, S. Lee, C. B. Park, K. Kang, *Green Chem.* **2017**, *19*, 2980.
[34] A. Petronico, K. L. Bassett, B. G. Nicolau, A. A. Gewirth, R. G. Nuzzo, *Adv. Energy Mater.* **2018**, *8*, 1.
[35] C. Karlsson, H. Huang, M. Strømme, A. Gogoll, M. Sjödin, *J. Electroanal. Chem.* **2014**, *735*, 95.

ADVANCED
SCIENCE NEWS

www.advancedsciencenews.com

ADVANCED
ENERGY & SUSTAINABILITY
RESEARCH
Open Access

www.advenergysustres.com

[36] M. Sterby, R. Emanuelsson, X. Huang, A. Gogoll, M. Strømme, M. Sjödin, *Electrochim. Acta* **2017**, *235*, 356.

[37] M. Sterby, R. Emanuelsson, F. Mamedov, M. Strømme, M. Sjödin, *Electrochim. Acta* **2019**, *308*, 277.

[38] K. Pirnat, G. Mali, M. Gaberscek, R. Dominko, *J. Power Sources* **2016**, *315*, 169.

[39] A. Ahmad, Q. Meng, S. Melhi, L. Mao, M. Zhang, B. H. Han, K. Lu, Z. Wei, *Electrochim. Acta* **2017**, *255*, 145.

[40] F. N. Ajjan, N. Casado, T. Rębiś, A. Elfwing, N. Solin, D. Mecerreyes, O. Inganäs, *J. Mater. Chem. A* **2016**, *4*, 1838.

[41] X. G. Li, H. Li, M. R. Huang, M. G. Moloney, *J. Phys. Chem. C* **2011**, *115*, 9486.

[42] M. R. Huang, S. J. Huang, X. G. Li, *J. Phys. Chem. C* **2011**, *115*, 5301.

[43] S. Huang, C. Min, Y. Liao, P. Du, H. Sun, Y. Zhu, A. Ren, *RSC Adv.* **2014**, *4*, 47657.

[44] S. Huang, C. Ma, Y. Liao, C. Min, P. Du, Y. Jiang, *J. Nanomater.* **2016**, *2016*, 1.

[45] S. Huang, P. Du, C. Min, Y. Liao, H. Sun, Y. Jiang, *J. Fluoresc.* **2013**, *23*, 621.

[46] Y. Liao, H. Wang, M. Zhu, A. Thomas, *Adv. Mater.* **2018**, *30*, 1.

[47] I. Gomez, O. Leonet, J. Alberto Blazquez, H. J. Grande, D. Mecerreyes, *ACS Macro Lett.* **2018**, *7*, 419.

[48] F. N. Ajjan, M. Vagin, T. Rębiś, L. E. Aguirre, L. Ouyang, O. Inganäs, *Adv. Sustain. Syst.* **2017**, *1*, 1700054.

[49] Z. Song, Y. Qian, M. L. Gordin, D. Tang, T. Xu, M. Otani, H. Zhan, H. Zhou, D. Wang, *Angew. Chem. Int. Ed.* **2015**, *54*, 13947.

[50] T. Kawai, K. Oyaizu, H. Nishide, *Macromolecules* **2015**, *48*, 2429.

[51] W. Choi, D. Harada, K. Oyaizu, H. Nishide, *J. Am. Chem. Soc.* **2011**, *133*, 19839.

[52] F. Xu, J. Xia, W. Shi, *Electrochem. Commun.* **2015**, *60*, 117.

[53] K. Oyaizu, H. Tatsuhira, H. Nishide, *Polym. J.* **2015**, *47*, 212.

[54] Y. Zhou, B. Wang, C. Liu, N. Han, X. Xu, F. Zhao, J. Fan, Y. Li, *Nano Energy* **2015**, *15*, 654.

[55] Y. Liang, Z. Chen, Y. Jing, Y. Rong, A. Facchetti, Y. Yao, S. Phadke, M. Cao, M. Anouti, B. Pan, J. Huang, Z. Feng, L. Zeng, M. He, L. Zhang, J. T. Vaughey, M. J. Bedzyk, P. Fenter, Z. Zhang, A. K. Burrell, C. Liao, *Adv. Energy Mater.* **2016**, *6*, 4956.

[56] S. Phadke, M. Cao, M. Anouti, *ChemSusChem* **2018**, *11*, 965.

[57] J. Bitenc, K. Pirnat, T. Bančič, M. Gaberšček, B. Genorio, A. Randon-Vitanova, R. Dominko, *ChemSusChem* **2015**, *8*, 4128.

[58] B. Pan, J. Huang, Z. Feng, L. Zeng, M. He, L. Zhang, J. T. Vaughey, M. J. Bedzyk, P. Fenter, Z. Zhang, A. K. Burrell, C. Liao, *Adv. Energy Mater.* **2016**, *6*, 2.

[59] S. Admassie, A. Elfwing, O. Inganäs, *Adv. Mater. Interfaces* **2016**, *3*, 1.

[60] E. Mitraka, M. J. Jafari, M. Vagin, X. Liu, M. Fahlman, T. Ederth, M. Berggren, M. P. Jonsson, X. Crispin, *J. Mater. Chem. A* **2017**, *5*, 4404.

[61] O. Bubnova, Z. U. Khan, H. Wang, S. Braun, D. R. Evans, M. Fabretto, P. Hojati-Talemi, D. Dagnelund, J. Arlin, Y. H. Geerts, S. Desbief, D. W. Breiby, J. W. Andreasen, R. Lazzaroni, W. M. Chen, I. Zozoulenko, M. Fahlman, P. J. Murphy, M. Berggren, X. Crispin, *Nat. Mater.* **2014**, *13*, 190.

[62] J. W. Thackeray, H. S. White, M. S. Wrighton, *J. Phys. Chem.* **1985**, *89*, 5133.

[63] G. Schiavon, S. Sitran, G. Zotti, **1989**, *32*, 209.

[64] A. J. Epstein, S. Etemad, A. F. Garito, A. J. Heeger, *Phys. Rev. B* **1972**, *5*, 952.

[65] Z. Khan, B. Senthilkumar, S. Lim, R. Shanker, Y. Kim, H. Ko, *Adv. Mater. Interfaces* **2017**, *4*, 1700059.

[66] C. H. Lai, D. Ashby, M. Moz, Y. Gogotsi, L. Pilon, B. Dunn, *Langmuir* **2017**, *33*, 9407.

[67] Z. Khan, B. Senthilkumar, S. Lim, R. Shanker, Y. Kim, H. Ko, *Adv. Mater. Interfaces* **2017**, *4*, 1.

[68] J. Luo, W. Zhong, Y. Zou, C. Xiong, W. Yang, *J. Power Sources* **2016**, *319*, 73.

[69] M. R. Arcila-Velez, M. E. Roberts, *Chem. Mater.* **2014**, *26*, 1601.

[70] M. Wagner, T. Rębiś, O. Inganäs, *J. Power Sources* **2016**, *302*, 324.

[71] M. Zeiger, D. Weingarth, V. Presser, *ChemElectroChem* **2015**, *2*, 1117.